Modified MWR Approach: Application to Agglomerative Precipitation

S. K. Bhatia and D. Chakraborty
Dept. of Chemical Engineering, Indian Institute of Technology, Powai, Bombay 400 076, India

A modified method of weighted residuals approach is presented that combines expansions based on limiting forms of the true solution to solve the population balance equation accurately for continuous agglomerative precipitation. A modified moment method is used that employs fractional moments and is stable for the infinite domain problem. Solutions are obtained for various values of the agglomeration parameter, and the results are fitted to Pade approximations providing simple relationships that can be used for data fitting, thus obviating further need to solve the population balance equation with a constant aggregation kernel. This method is applied to experimental data on the precipitation of nickel ammonium sulfate and calcium carbonate to yield kinetic parameters.

Introduction

The method of weighted residuals (MWR) is one of the prime techniques used in chemical engineering for the solution of boundary value and a variety of other problems (Finlayson, 1972). For an equation of the form,

$$q = Aq + f, \tag{1}$$

the solution is accomplished by providing the unknown q with a satisfactory finite dimensional approximation on a Hilbert space $\mathcal{H}$ on which the operation A is defined. For this we express the solution q as the linear combination:

$$q(y) = \sum_{i=1}^{N} a_i \varphi_i(y) \tag{2}$$

in which the trial functions φ_i are derived from a complete set forming a basis in $\mathcal{H}$. The unknown coefficients a_i are now estimated by orthogonalizing the residual in Eq. 1 with respect to a suitably chosen set of functions. When these functions are chosen from the sequence y^j, $j=0, 1, \ldots, N-1$, the technique is known as the method of moments; when they are obtained from the sequence $\varphi_i(y)$, the well known Galerkin method results. Orthogonal polynomials form the most common choice for $\varphi_i(y)$, a consequence of Wierstrass' theorem (Dennery and Krzywicki, 1967) and the attendant algebraic simplicity, and the moment and Galerkin methods then become equivalent. When the orthogonalizing functions form the sequence $\delta(y-y_i)$ where y_is are the roots of an appropriate polynomial φ_i, the method is known as the collocation technique.

While the above method is often successful, in many cases a large number of terms are required with attendant high demands on computer time. This occurs particularly in problems where there are local steep gradients in $q(y)$ or where this function assumes distinctly different shapes in different regions. For such cases, it is often desirable to partition the domain into several regions with a different polynomial approximation in each region (Finlayson, 1980). Another alternative, often more convenient, is offered by Ramkrishna (1973) through the use of problem-specific polynomials (PSP). In this method, a suitably truncated version of Eq. 1 is first solved analytically, and the solution $q^*(y)$, believed to be a first approximation to the true solution $q(y)$, is used to construct the latter by:

$$q(y) = q^*(y) \sum_{i=1}^{N} a_i \varphi_i(y) \tag{3}$$

with the polynomials φ_i being orthogonalized with weight function $q^*(y)$. In practice, however, it often is not possible to find a single analytically solvable truncation of Eq. 1 that yields a functional form $q^*(y)$ which is adequate over the whole domain, and further modifications are necessary. Thus, Sampson and Ramkrishna (1985) have suggested the use of root

shifted PSPs to improve on an earlier solution of Singh and Ramkrishna (1975) for the Brownian coagulation problem. In this article, a simpler procedure that uses different limiting solutions obtained from two separate truncations of Eq. 1 is described and shown to be useful in solving the population balance equation (PBE).

The particular equation solved is the PBE for simultaneous nucleation, growth and agglomeration of particles in a well mixed continuous precipitator, given in dimensionless form as:

$$\frac{dq}{dy}+q(y)=\frac{\phi}{2}y^2\int_0^y\frac{q(\lambda)q([y^3-\lambda^3]^{1/3})}{(y^3-\lambda^3)^{2/3}}\,d\lambda - \phi q(y)\int_0^\infty q(\lambda)d\lambda \quad (4)$$

$$q(0)=1 \quad (5)$$

which assumes a constant agglomeration kernel as well as conservation of particle shape on agglomeration. Since this is the simplest case, the above equation has been preferred by numerous investigators for the interpretation of measured particle size distributions (Lamey and Ring, 1986; Hounslow et al., 1988; Marchal et al., 1988; Hounslow, 1990). However, even the constant agglomeration kernel case in Eq. 4 is difficult to solve accurately, and this has prompted researchers to seek more approximate solutions. Thus, Lamey and Ring simplify the model by assuming aggregation to be length-conserving, rather than volume-conserving, while others (Hounslow et al., 1988; Marchal et al., 1988; Hounslow, 1990) use a finite domain approximation. The latter simplification has been found (Gelbard and Seinfeld, 1978) to yield unacceptably large errors unless the domain is sufficiently wide, which usually is not known *a priori*. Further, in many of the methods, the procedure is not derived from any version of the MWR, but is based on discretizations suggested by intuitive or other less rigorous considerations. Chang and Wang (1984a,b) have suggested a shifted Legendre polynomial approach with the Galerkin method, but the technique is not free from finite domain error. This error is avoided by Singh and Ramkrishna (1977) for the binary breakage problem in their application of the PSP method. For the aggregation problem, however, no single truncation yields a suitable PSP, as evident from the work of Sampson and Ramkrishna (1985).

An important feature of most earlier MWR-based solutions of the PBE is that they have not used the moment procedure in orthogonalizing the residual. The latter procedure may be advantageous as it yields the moments accurately so that mass and number balances on the system are satisfied. In addition, in calculating mass-averaged particle size and variance of the size distribution based on particle mass it is necessary to solve for the moments up to the fifth (that is, the first six) moments. To obtain these moments accurately the tail of the distribution (at large y) needs to be accurately known, requiring an unreasonably large number of terms in the expansion of $q(y)$ in Eq. 2 if a procedure, other than a moment-based one, is chosen. When the latter method is used in satisfying the residual, an arbitrary number of moments of $q(y)$ may be estimated accurately with fewer terms and negligible compromise in the accuracy of the computed $q(y)$. However, on an infinite domain the moment method becomes unstable with increasing number of moments as this requires more of the tail to be accurately represented by the expansion in Eq. 2. Avoidance of this instability in the moment method therefore is of concern in using this technique.

Perhaps a simpler version among the developments noted above is that of Hounslow (1990), which is attractive at the same time in that the first four moments are conserved so that mass and number balances are maintained. This method considers N_1 subintervals with the boundary points satisfying:

$$y_{i+1}=ry_i, \qquad i=1,2,\ldots,N_1 \quad (6)$$

and solves for the dimensionless number of particles Q_i in each subinterval given by:

$$Q_i=\int_{y_i}^{y_{i+1}}q(y)dy, \qquad i=1,2,\ldots,N_i \quad (7)$$

While developed for any aggregation kernel for the case considered here, Hounslow's formulation can be expressed as the system of equations:

$$1-Q_1\left(1+\phi\sum_{i=1}^{N_1}Q_i\right)+\frac{2}{(1+r)y_1}\left(Q_1-\frac{r}{r^2-1}Q_2\right)=0 \quad (8)$$

$$\phi\left[Q_{i-1}\sum_{j=1}^{i-2}2^{j-i+1}Q_j+\frac{1}{2}Q_{i-1}^2-Q_i\sum_{j=1}^{i-1}2^{j-i}Q_j-Q_i\sum_{j=i}^{N_1}Q_j\right] + \frac{2}{(1+r)y_i}\left[\frac{r}{r^2-1}Q_{i-1}+Q_i-\frac{r}{r^2-1}Q_{i+1}\right]-Q_i=0. \qquad i=2,3,\ldots,N_1 \quad (9)$$

which must be solved simultaneously to obtain the quantities Q_i, where $i=1,2,\ldots,N_1$. The ratio of successive interval sizes r is taken as $2^{1/3}$. As such, the method is unstable, yielding fluctuating values of the Q_is. To stabilize the method, Eq. 8 is modified to (Smit, 1991; Hostomsky and Jones, 1991):

$$1-Q_1\left(1+\phi\sum_{j=1}^{N_1}Q_i\right)-\frac{2}{(1+r)(r^2-1)y_1}(Q_1+rQ_2)=0 \quad (10)$$

in which an extra term $[-2r^2Q_1/y_1(r+1)(r^2-1)]$ is added to conserve the total number. This, however, leads to some errors in the distribution, particularly at large y_1 and consequently in the higher moments. Thus, when moments higher than the third are required, the procedure is likely to be inaccurate.

As noted above, the present work is aimed at adapting the PSP method by combining the results obtained from different truncations for the solution of Eq. 4. In addition, a modification of the moment method is used that avoids the instability while yielding accurately the solution as well as its moments to any desired order. The method, which avoids the finite domain error, is shown to be more accurate than that of Hounslow (1990) at large y_1, and empirical curve fits of the general solution, in terms of the parameter ϕ, are obtained obviating any further need to solve Eq. 4. The empirical expressions are easy to use and applied to the interpretation of experimental particle size distributions.

Numerical Procedure

In developing the numerical procedure adopted here, we first integrate Eq. 4 over the domain $0 \le y < \infty$ to obtain the zeroth moment:

$$\mu_0 = \int_0^\infty q(y)dy = \frac{(\sqrt{1+2\phi}-1)}{\phi} \tag{11}$$

Expressions for the higher moments, however, cannot be obtained analytically. Defining the new variable:

$$\alpha = \frac{1}{\sqrt{1+2\phi}} \tag{12}$$

provides the transformed population balance equation:

$$\alpha \frac{dq}{dy} + q(y) = \frac{1-\alpha^2}{4\alpha} y^2 \int_0^y \frac{q(\lambda)q[(y^3-\lambda^3)^{1/3}]}{(y^3-\lambda^3)^{2/3}} d\lambda \tag{13}$$

upon combining Eqs. 4, 11, and 12. Equation 13 may be formally integrated to yield the integral equation:

$$q(y) = e^{-y/\alpha}\left[1 + \frac{(1-\alpha^2)}{4\alpha^2}\int_0^y y'^2 e^{y'/\alpha} \times \int_0^{y'} \frac{q(\lambda)q[(y^3-\lambda^3)^{1/3}]}{(y'^3-\lambda^3)^{2/3}} d\lambda dy'\right] \tag{14}$$

which we shall solve by a moment technique. We take the jth moment of Eq. 14 to obtain:

$$\mu_j = \alpha^{j+1}\Gamma(j+1) + \frac{(1-\alpha^2)}{4\alpha^2}\int_0^\infty q(\lambda)\int_0^\infty q(z)\int_0^\infty [s+(z^3+\lambda^3)^{1/3}]^j e^{-s/\alpha} ds dz d\lambda \tag{15}$$

where

$$\mu_j = \int_0^\infty y^j q(y)dy \tag{16}$$

and it is understood that j can assume fractional as well as integral values. The normal course of solution would now be to provide a Hilbert space setting for $q(y)$ by expanding it in terms of an appropriate polynomial sequence. Ideally, to generate this sequence a reasonable approximation to $q(y)$ is desirable, as problem-specific polynomials may be generated following Ramkrishna (1973). However, the nonlinear nature of Eq. 13 or 14 makes the construction of such an approximation difficult if not impossible. Neglect of the nonlinear term in Eq. 13 yields:

$$q_L(y) = e^{-y/\alpha} \tag{17}$$

which from Eq. 14 is easily recognized to be a lower bound for $q(y)$. This limiting solution, however, is a good approximation for sufficiently small y ($y \ll \alpha$), a feature evident from the scaling:

$$\xi = \frac{y}{\alpha} \tag{18}$$

which transforms Eq. 14 to:

$$q(\xi) = e^{-\xi}\left[1 + \frac{(1-\alpha^2)}{4}\int_0^\xi \xi'^2 e^{\xi'} \times \int_0^{\xi'} \frac{q(\xi')q[(\xi'^3-\lambda^3)^{1/3}]d\lambda d\xi'}{(\xi'^3-\lambda^3)^{2/3}}\right] \tag{19}$$

showing that for ξ sufficiently small, the term involving the integral will be negligible. For $\alpha \to 1$ (that is, $\phi \to 0$), the limiting solution in Eq. 17 approaches the exact pure growth result:

$$q_u(y) = e^{-y} \tag{20}$$

which is obtained from the truncation of Eq. 4, in which the aggregation terms are neglected. Clearly, Eq. 17 may be expected to provide a satisfactory PSP for our PBE in the neighborhood of $\alpha = 1$ (that is, small ϕ). Our interest, however, lies in the region of significant agglomeration effects, in which $\phi = 0(1)$ or larger so that α is small. The choice of either $q_L(y)$ or $q_u(y)$ for $q^*(y)$ in the expansion in Eq. 3, in the region $\phi \ge 5$, did not yield convergence with oscillations in $q(y)$ for N as large as 12. In these computations, an adaptation of the moment method to be subsequently discussed, in which j can assume fractional values, was used. In addition, the Vorobyev method, as outlined by Singh and Ramkrishna (1973), with $q_L(y)$ or $q_u(y)$ as the starting trial vector φ_1, in combination with our moment method, was also unsuccessful.

In searching for suitable approximations to $q(y)$, while $q_L(y)$ is satisfactory for small y, it was found from computations using Hounslow's method that for large y the solution was of the same order of magnitude as $q_u(y)$. This was confirmed for values of ϕ as large as 1,000. This leads to the order of magnitude approximation:

$$q(y) = 0(e^{-y}) \tag{21}$$

for large y that has similar functional form as $q_u(y)$. Having obtained the forms of the solution for small and large y we now write:

$$q(y) = e^{-y/\alpha}\sum_{i=1}^N a_i' \varphi_i(y) + e^{-y}\sum_{i=1}^N b_i' \varphi_i'(y) \tag{22}$$

which provides the benefit of both limits. The functions $\varphi_i(y)$ and $\varphi_i'(y)$ as usual form polynomial sequences, and for convenience we have used the same number of terms N in each summation although this is clearly not mandatory. An earlier attempt at combining limiting solutions has been made by Sampson and Ramkrishna (1985) for the Brownian coagulation problem, but an expansion around the small y solution was not considered.

In the actual implementation of the procedure we rewrite Eq. 22 as:

$$q(y) = e^{-y/\alpha}\sum_{i=1}^N a_i y^{i-1} + e^{-y}\sum_{i=1}^N b_i y^{i-1} \tag{23}$$

which is the form of $q(y)$ used in solving Eq. 14. Substitution of Eq. 23 into Eqs. 15 and 16 provides a system of $2N-1$ equations for $2N-1$ appropriately chosen values of j. An additional relation is provided by Eq. 5 which yields:

$$a_1 + b_1 = 1 \tag{24}$$

The procedure thus provides a system of $2N$ equations in the $2N$ unknowns that comprise the N a's and N b's. The system may be solved using any of the known methods for nonlinear algebraic equations.

For computing the integrals in the second term of Eq. 15 Gauss-Laguerre quadrature may be used; however, the steep distributions $q(y)$ for small values of α would necessitate a very large number of points. To alleviate this difficulty it is expedient to divide the domain $0 \le y \le \infty$ into N_s elements. For the first $N_s - 1$ elements, each element spans the subdomain $y_{a_i} \le y \le y_{a_{i+1}}$, so that $y_{a_1} = 0$. The last (N_sth) element spans the region $y_{aN_s} \le y < \infty$. Each of the first $N_s - 1$ elements is now rescaled as:

$$y = y_{a_i} + \Delta y_i x, \qquad y_{a_i} \le y \le y_{a_{i+1}} \tag{25}$$

where

$$\Delta y_i = y_{a_{i+1}} - y_{a_i}, \qquad i = 1,2, \ldots, N_s - 1 \tag{26}$$

so that $0 \le x \le 1$. Integrals over the region $0 \le x \le 1$ are now evaluated by an M point Gauss-Legendre quadrature. The last (or N_sth) element is rescaled as:

$$y = y_{aN_s} + z \tag{27}$$

so that $0 \le z \le \infty$. Integrals over this region are now evaluated by means of an M-point Gauss-Laguerre quadrature.

The specification of the $2N-1$ values of j forms an important part of the procedure. The usual practice in using the method of moments would be let j take on the integer values $0,1,2, \ldots, 2N-2$. However, with increase in N the highest moment also increases, and in an infinite domain this destabilizes the procedure unless the integrals are calculated very accurately with a large number of quadrature points. A more efficient approach is to seek more fractional or smaller moments with a fixed maximum moment as N is increased. Thus, if it is desired to solve accurately the PBE only up to the Lth moment, the strategy is to choose equally spaced $2N-1$ values of j in $[0, L]$. Then,

$$j = \frac{(i-1)L}{(2N-2)} \qquad i = 1,2, \ldots, 2N-1 \tag{28}$$

and this way as N is increased more fractional or smaller moments are taken with L fixed, and there is lesser tendency for the procedure to become unstable.

Results and Discussion

Numerical convergence

As mentioned above, Eqs. 15, 16, 23 and 24 form a system of $2N$ nonlinear algebraic equations in the N a_i's and N b_i's,

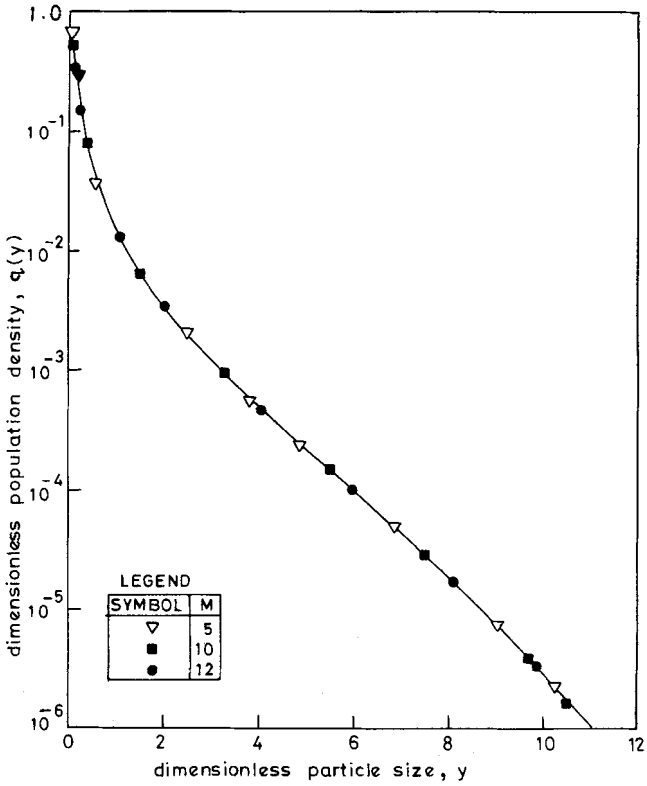

Figure 1. Convergence behavior of solution to population balance equation with variation in number of quadrature points at $\phi = 100$.

$L = N = 4$ and $N_s = 7$. Element locations are 0, 0.05, 0.25, 2, 5, 8, and 14.

and these were solved using the Levenberg-Marquardt algorithm as implemented in the IMSL subroutine NEQNF. Since for small y the solution is expected to be close to the lower bound in Eq. 17, the starting guess solution may be taken as $a_1 = 1$, $a_i = 0$, $i = 2, \ldots, N$ and $b_i = 0$, $i = 1, \ldots, N$. In the actual computations the value of ϕ was progressively decreased with the results from one run being used as the guess for the subsequent value of ϕ. A relative tolerance of 10^{-7} (the relative difference between successive approximations) was used as the stopping criterion. Computations were performed on a CDC CYBER 180 series main-frame computer, and the convergence of the solution was obtained in 50 to 100 seconds when results from a prior value of ϕ were used as the starting guess with the precise value depending on the magnitudes of ϕ.

Figure 1 shows the dimensionless population density at $\phi = 100$ with $N = L = 4$ and three different values of M (the order of the quadrature), showing that convergence has been achieved for $M = 5$ or above at least over 6 orders of magnitude in $q(y)$. In the computations, the value of N_s was taken as 7 with element boundaries at $y_a = 0$, 0.05, 0.25, 2, 5, 8, 14. On this plot, sufficiently accurate convergence of the integrations is apparent with the variation in $q(y)$ being within 2% on increasing M from 5 to 12. Although the results are not shown in the figure, calculations with other values of M between 5 and 12 also yielded the same results as in Figure 1 consistent with the conclusion of convergence. Figure 1 also shows the steep decline in $q(y)$ for small y as is to be expected from the

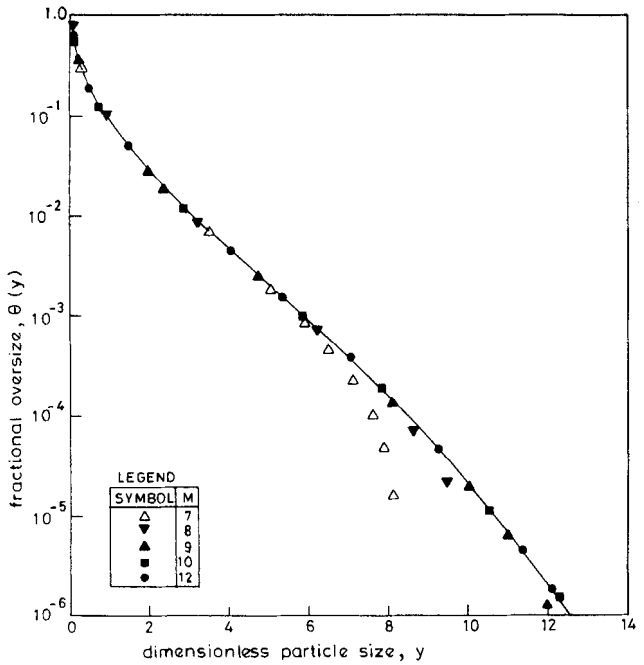

Figure 2. Convergence behavior of the fractional oversize with variation in number of quadrature points at $\phi = 100$.

$L = N = 4$ and $N_s = 7$. Element locations are the same as in Figure 1.

recognition that in this region $q(y)$ is close to its lower bound in Eq. 17.

In utilizing the solutions to the PBE it may be noted that experimental data are generally available in the form of fractional oversize values, and it is therefore important to examine the convergence of this distribution. Analytical integration of Eq. 23 provides:

$$\Theta(y) = \frac{1}{\mu_0} \sum_{i=1}^{N} (i-1)! \sum_{k=0}^{i-1} (a_i \alpha^{i-k} e^{-y/\alpha} + b_i e^{-y}) \frac{y^k}{k!} \tag{29}$$

and having solved for a_i and b_i, $i = 1, \ldots, N$, for a given value of ϕ, it is now straightforward to obtain the oversize distribution. Figure 2 shows this distribution for $\phi = 100$ and various values of M, with other numerical parameters being the same as in Figure 1. Interestingly, the figure shows that convergence within a few percent over 6 orders of magnitude in the fractional oversize requires at least 10 quadrature points, even though the population density has converged to 6 orders for as few as 5 quadrature points per element (c.f. Figure 1). To explain this behavior we consider the definition of the fractional oversize given $q(\lambda)$ for $\lambda \le y$:

$$\tilde{\theta}(y) = 1 - \frac{1}{\mu_0} \int_0^y q(\lambda) d\lambda \tag{30}$$

and study the influence of a small fractional error of magnitude Δ in the computation of the integral in Eq. 30 while maintaining the total number balance. From Eq. 30 we now readily obtain the absolute error in the computed value of the oversize $\theta(y)$ as:

$$|\theta(y) - \tilde{\theta}(y)| = \Delta[1 - \tilde{\theta}(y)] \tag{31}$$

which implies that for large y [for which $\tilde{\theta}(y) \ll 1$] the absolute error in $\theta(y)$ can be as large as Δ. Thus, for given N to obtain an accuracy of within 5% in $\theta(y)$ when $\tilde{\theta}(y)$ is of the order of 10^{-6} it is necessary that Δ [and hence the fractional error in $q(\lambda)$] be less than 5×10^{-8}. This is a very stringent requirement and necessitates a sufficiently large number of quadrature points in the evaluation of the integrals in Eq. 15 as well as a conservative tolerance in solving the algebraic equations for the a_i's and b_i's. It can be explained more directly if we rewrite Eq. 30 as:

$$\tilde{\theta}(y) = \frac{1}{\mu_0} \int_y^{\infty} q(\lambda) d\lambda \tag{32}$$

from which it is obvious that convergence of $\tilde{\theta}(y)$ requires convergence of the population density $q(\lambda)$ for values of λ significantly larger than y.

Essentially the same results as in Figure 2 for $M = 12$ were also obtained when the tolerance parameter for the solution of the algebraic equations was reduced to 10^{-8} or 10^{-9}, consistent with the conclusion of convergence at the 10^{-6} level for $\theta(y)$. It, however, is also necessary to check convergence with respect to N. Figure 3 shows the convergence of the fractional oversize curve with respect to variation in the number of terms in the expansion, N, for $M = 12$ and $L = 5$. Essentially the same results are obtained in all three cases, though at the 10^{-6} level the result for $N = 4$ is about 20% lower than that for $N = 5$ or 6. Convergence at this level has therefore occurred for $N \ge 5$. Similar results are obtained for $L = 4$ for a larger number of collocation points and $N \ge 5$. It is therefore apparent that the

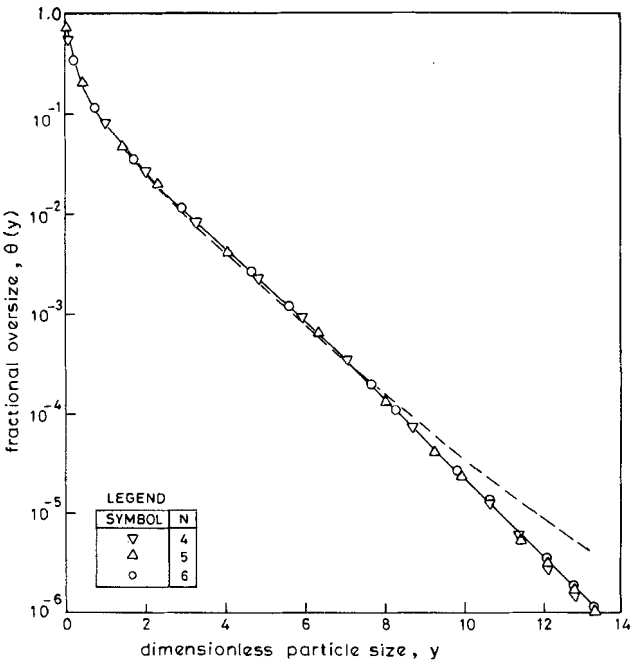

Figure 3. Convergence of fractional oversize with respect to variation in N at $\phi = 100$.

$M = 12$, $L = 5$ and $N_s = 7$. Element locations are the same as in Figure 1. Dashed curve represents solution with Hounslow's method.

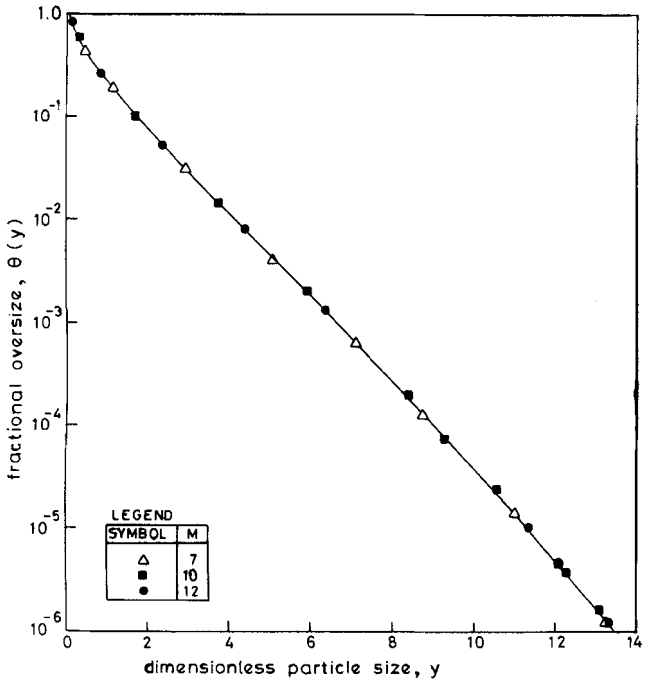

Figure 4. Convergence of fractional oversize with variation in M at $\phi = 5$.

$L = N = 4$ and $N_s = 7$. Element locations are the same as in Figure 1.

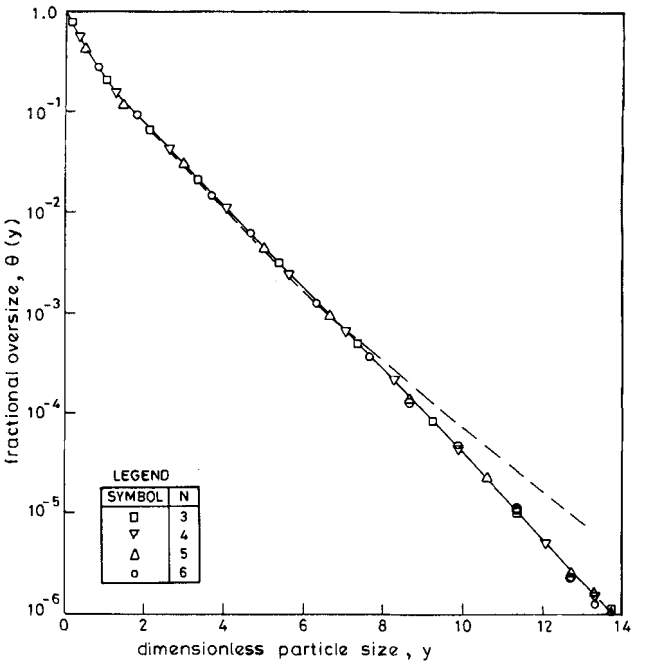

Figure 5. Convergence of fractional oversize with variation in N at $\phi = 5$.

$L = 5$, $M = 12$, and $N_s = 7$. Element locations are the same as in Figure 1. Dashed curve represents solution with Hounslow's method.

solution in Figure 3 for $\phi = 100$ is accurate to within a few percent ($< 5\%$) at the 10^{-6} level. Also superimposed on Figure 3 is the solution from Hounslow's method with 50 equations and $y_1 = 0.002$. The latter solution is sufficiently accurate only to the 10^{-4} level, deviating by a factor of 3 to 4 at the 10^{-6} level. However, it is about 3–5 times faster than the current method. To achieve the same level of accuracy the number of equations in Hounslow's method would have to be increased substantially making it no longer attractive. In addition, the workspace required for solving a much larger system of equations would be prohibitive.

Figure 4 shows that for a lower value of the agglomeration parameter of $\phi = 5$, convergence of the oversize distribution $\theta(y)$ is obtained for $M > 7$ even at the 10^{-6} level with $L = N = 4$ and $N_s = 7$. Essentially the same results are also obtained with $L = 5$ when the convergence of N is examined with $M = 12$. Figure 5 indicates that at this value of ϕ, convergence at the 10^{-6} level is obtained for $N > 3$. Also superimposed is the solution from Hounslow's method (with 50 equations and $y_1 = 0.002$), which is now accurate to only the 10^{-3} level and shows a several-fold deviation at the 10^{-6} level.

When the present solution is compared with that of Hounslow's method, the latter tends to not only overpredict significantly the oversize fraction at large y, but also underpredict somewhat at intermediate values of y. All the computations of Hounslow's method were done with $N_1 = 50$ (that is, 50 equations) and $y_1 = 0.002$ as suggested by Smit (1991). These values are consistent with the range identified by Hounslow (1990) for negligible error but for the case of pure growth. In the presence of aggregation, however, there appears no obvious way of identifying suitable values of these variables. Nevertheless, firm evidence of the overprediction at large y and underprediction at intermediate values of y is also obtained from Hounslow's solution at $\phi = 0$, for which the exact solution of $\theta(y)$ is given by $q_u(y)$ as in Eq. 20.

Figure 6 shows the solutions obtained with 50 equations and $y_1 = 0.002$ and $y_1 = 0.0002$, both of which are consistent with the range suggested by Hounslow (1990). The several-fold overprediction even at the 10^{-5} level of oversize fraction is evident

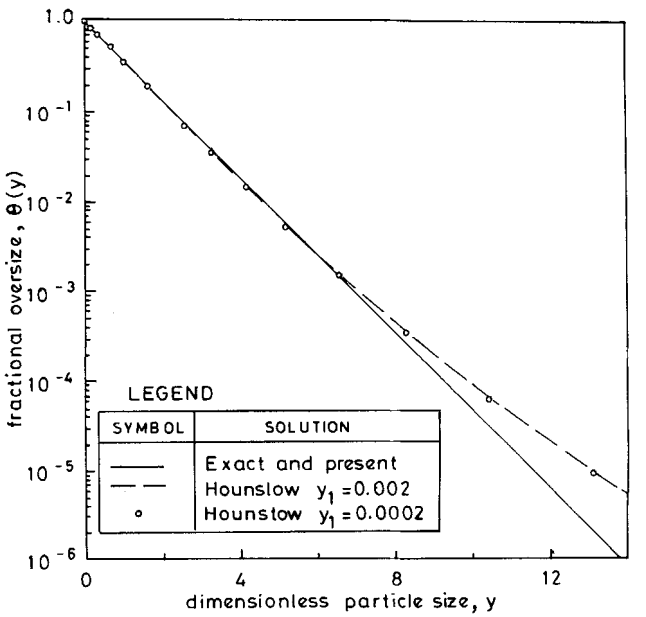

Figure 6. Comparison of solutions from present and Hounslow's methods with exact result for $\phi = 0$.

in the figure. Further, the variable y_1 does not seem to materially improve the overprediction even when increased tenfold. Even with 70 equations the results were the same as in Figure 6, indicating the difficulty of obtaining convergence and improved predictions. It would appear from these findings that the discretization of the growth-related derivative term dq/dy over the finite domain approximation to the original infinite domain is responsible for this error. Nevertheless, since sufficiently accurate experimental data for oversize fraction are generally available to only the 10^{-4} level, Hounslow's technique, by virtue of its speed of solution, remains a powerful option for the fitting of experimental data. Due to the enhanced workspace requirements, we could not use Hounslow's method for sufficiently large number of equations to obtain significantly better accuracy. It, however, should be noted that our solution as given by Eq. 23 exactly matches $q_u(y)$ for $\phi = 0$ and falls along the solid line on the semilogarithmic coordinates of Figure 6. It may be mentioned that for low ϕ (that is, $\alpha \rightarrow 1$), since $q_u(y)$ and $q_L(y)$ approach each other, an additional condition $b_1 = 0$ is substituted for the last of the moment equations in Eq. 15.

Another interesting feature of Figures 2–5 is the existence of a point of inflection in the fractional oversize plots on the semilogarithmic coordinates used, for the present solution, but not for Hounslow's. By differentiating $\ln[\theta(y)]$ twice it is easily seen that a point of inflection will exist when:

$$q = -\theta\mu_0 \frac{d\ln(q)}{dy} \tag{33}$$

For example, such conditions are easily seen to be met at about $y = 4$ for $\phi = 100$ from estimation of the values of q, θ and $d\ln(q)/dy$ in Figures 1 and 3 and of μ_0 from Eq. 11. The inflection at $y = 4$ is evident for our solution in Figure 3, but not for Hounslow's. Nevertheless, in this region the predicted fraction oversize for the two solutions are very nearly the same. It may be noted that there exist data in the literature (for example, Lamey and Ring, 1986) that show such points of inflection, in fact, even stronger ones that most likely indicate a different aggregation kernel from the constant one of this work.

General solution

Among the various kernels listed by Hartel and Randolph (1986), the constant agglomeration kernel considered here is the simplest and consequently preferred by most investigators. However, due to numerical difficulties and the large computational time requirement in obtaining accurate solutions, the fitting of experimental data is still difficult and earlier investigators had to simplify the aggregation model even further (Tavare et al., 1985). It was therefore sought in this work to obtain general solutions of Eqs. 4 and 5 for various values of the single parameter ϕ, using the method developed here. Figures 7 and 8 show the number density and fractional oversize curves for various values of ϕ in the range [0, 250]. These curves were obtained with $L = N = 5$, $N_s = 7$ (same element locations as in Figure 1) and $M = 12$ for $\phi \leq 100$, while $M = 15$ for $\phi > 100$. These numerical parameters were found to give accuracy to within a few percent ($< 5\%$) at the 10^{-5} level over the whole range of ϕ. Since for $\phi = 0$ the solution is analytical,

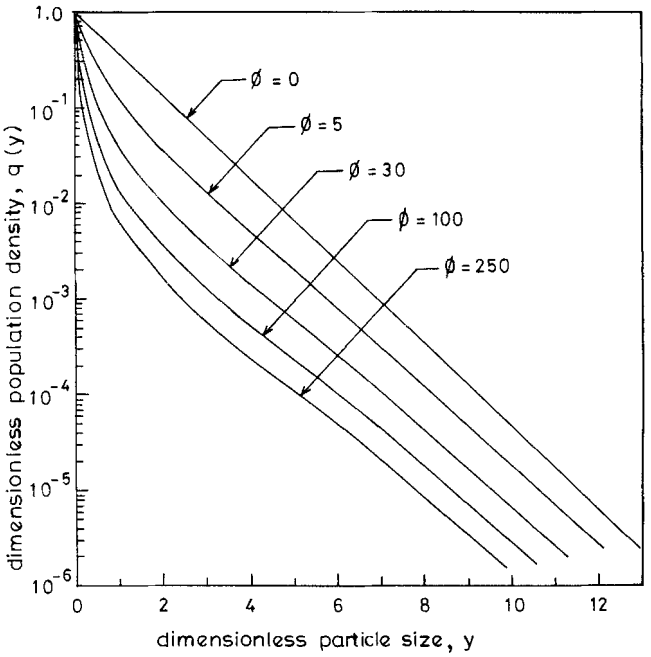

Figure 7. Population density distributions for various values of aggregation parameter ϕ.

is analytical, the computations were performed only for $\phi \geq 2$. It may be noted in Eq. 23 that as $\phi \rightarrow 0$, $\alpha \rightarrow 1$ and the two exponentials approach each other. Thus, the two terms are no longer distinct, and it becomes necessary to use the condition $b_1 = 1$ in place of the last of the moment equations. However, no problem was faced for ϕ as low as 2.

To facilitate data fitting it was decided to obtain empirical curve fits for the calculated oversize distributions, since these are generally more accurately known from experiment than the number density distributions. To this end, the results for

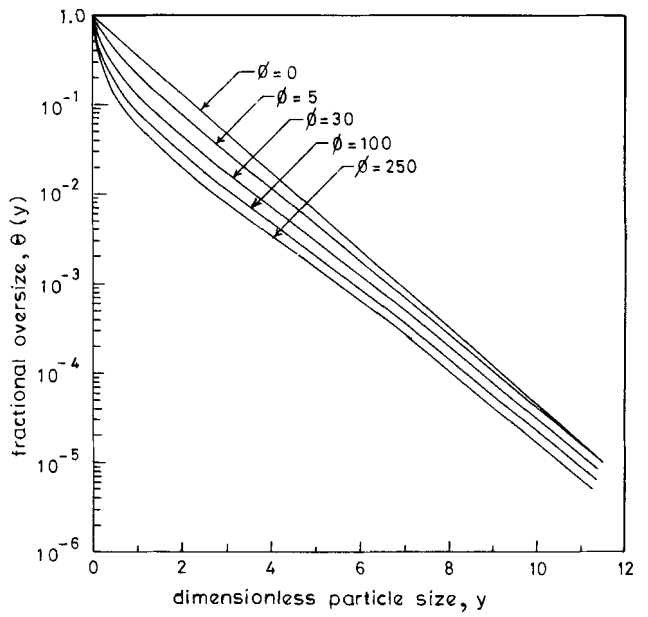

Figure 8. Fractional oversize distributions for various values of aggregation parameter ϕ.

Table 1A. Values of Constants in Eq. 34

Cum. oversize	d_1	d_2	d_3	d_4	d_5
1×10^{-5}	1.55272×10^{-3}	4.09394×10^{-2}	6.03963×10^{-10}	3.70681×10^{-3}	2.31041×10^{-5}
5×10^{-5}	-1.68317×10^{-3}	3.07217×10^{-2}	9.02938×10^{-8}	3.28258×10^{-3}	2.01544×10^{-5}
1×10^{-4}	-2.77976×10^{-3}	3.59676×10^{-2}	4.38568×10^{-9}	4.15786×10^{-3}	3.21447×10^{-5}
5×10^{-4}	1.54371×10^{-2}	1.85758×10^{-1}	6.27712×10^{-9}	2.57408×10^{-2}	2.00145×10^{-3}
1×10^{-3}	-9.93259×10^{-3}	8.16947×10^{-1}	-5.40774×10^{-8}	1.11856×10^{-1}	8.03594×10^{-3}
4×10^{-3}	-5.5697×10^{-3}	3.15242×10^{-1}	9.00008×10^{-11}	5.89328×10^{-2}	2.7925×10^{-3}
7×10^{-3}	-1.03855×10^{-2}	5.2858×10^{-1}	9.98128×10^{-8}	1.06646×10^{-1}	7.14452×10^{-3}
0.01	-1.21255	3.59004×10^{-1}	1.80643×10^{-6}	-4.79723×10^{-1}	2.95553×10^{-1}
0.02	9.88783×10^{-2}	-2.59599×10^{-2}	9.14966×10^{-5}	3.74884×10^{-2}	-4.73336×10^{-3}
0.04	-2.26931×10^{-1}	5.03691×10^{-2}	-1.10673×10^{-1}	4.26078×10^{-2}	3.179×10^{-2}
0.07	7.37464×10^{-1}	-6.31381×10^{-2}	2.28031×10^{-1}	9.22762×10^{-2}	-7.87704×10^{-3}
0.09	4.03024×10^{-1}	-4.93141×10^{-2}	1.11064×10^{-1}	1.0552×10^{-1}	-9.86744×10^{-3}
0.1	-2.39826×10^{-1}	1.59965×10^{-3}	-2.06911×10^{-1}	1.7166×10^{-1}	-3.20655×10^{-2}
0.2	8.65313×10^{4}	3.47793×10^{3}	4.94269×10^{4}	1.51619×10^{4}	2.94699×10^{2}
0.4	8.90012×10^{-2}	-2.39153×10^{-2}	-1.91522×10^{-1}	5.84898×10^{-1}	-5.78383×10^{-2}
0.7	2.79281×10^{3}	1.6872×10^{2}	7.09365×10^{3}	3.68732×10^{3}	8.55916×10^{1}
0.9	8.0049×10^{15}	5.469×10^{16}	2.476×10^{17}	1.00001×10^{10}	5.53413×10^{17}

$\phi(y)$ from the present method were used first to obtain y vs. ϕ data at fixed values of the cumulative oversize θ. These y vs. ϕ data were then fitted using least squares by expressions of the form:

$$y=\frac{1+d_1\phi^p+d_2\phi^{2p}}{\{[-1/\ln(\theta)]+d_3\phi^p+d_4\phi^{2p}+d_5\phi^{3p}\}} \tag{34}$$

yielding y-ϕ contours of constant fractional oversize θ. Tables 1a and 1b give the constants d_1-d_5 and p for various values of the fractional oversize θ, in the range $10^{-5}\le\theta\le1$. For these constants, Eq. 34 was found to yield y values accurate to within 1-2% of the original ones. Given any arbitrary value of ϕ, Eq. 34 can now be used to obtain $\theta(y)$ curves accurately in the form of (y, θ) data at the specific θ values in Table 1. To fit experimental data it is now only necessary to interpolate between the above (y, θ) data at the experimental y's. Figure 9 shows the adequacy of the present approximation at some arbitrary values of ϕ, which were not used in obtaining the values of the constants in Table 1.

In interpreting experimental data it often is necessary to estimate the third moment μ_3 defined by:

Table 1B. Values of Constants in Eq. 34

Cumulative Oversize	p
1×10^{-5}	0.4372
5×10^{-5}	0.4612
1×10^{-4}	0.4440
5×10^{-4}	0.2225
1×10^{-3}	0.2831
4×10^{-3}	0.39777
7×10^{-3}	0.39885
0.01	0.0235
0.02	0.23122
0.04	0.1347
0.07	0.33771
0.09	0.30548
0.1	0.19694
0.2	0.55087
0.4	0.28403
0.7	0.63762
0.9	0.40692

$$\mu_3=\int_0^\infty y^3q(y)dy \tag{35}$$

Figure 10 shows the computed third moment as a function of the agglomeration parameter ϕ. For use in data fitting, this curve was fitted, using least squares, to the expression:

$$\mu_3(\phi)=6\left[\frac{1+C_1\phi^m+C_2\phi^{2m}}{1+C_3\phi^m+C_4\phi^{2m}+C_5\phi^{3m}}\right] \tag{36}$$

and Table 2 gives the values of the constants C_1-C_5 and m.

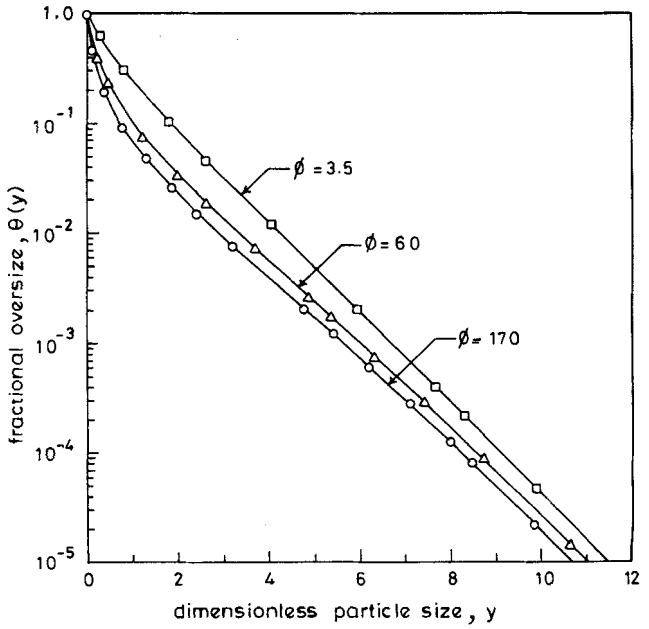

Figure 9. Fractional oversize distributions obtained from Eq. 34 with actual numerical solution of PBE for arbitrary values of ϕ.

Curves represent Eq. 34 and symbols the actual solutions.

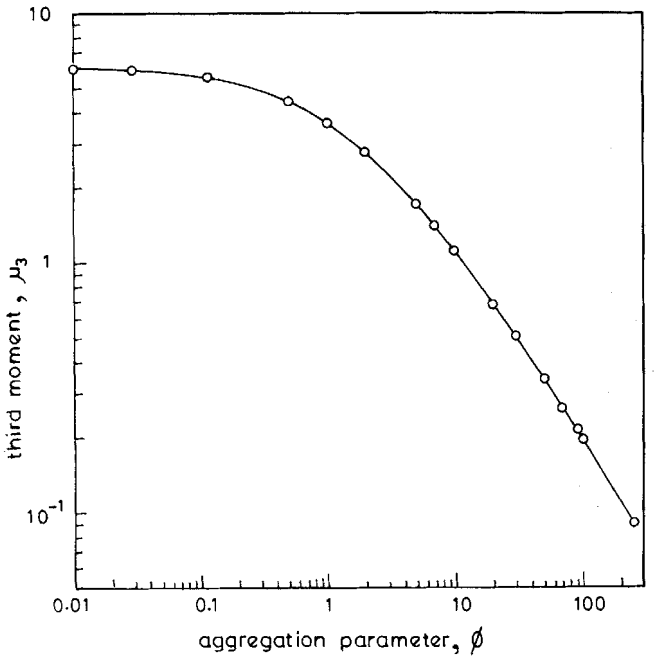

Figure 10. Variation of third moment of population density, μ_3, with aggregation parameter ϕ.

Curve represents Eq. 36 and the symbol actual values.

Application to experimental data

A convenient route to interpreting experimental particle size distribution data from an MSMPR precipitator by means of the model of Eqs. 4 and 5 would be to obtain by nonlinear regression the parameters ϕ and $G\tau$ so that the predicted value of $\theta(\ell/G\tau)$ matches the measured cumulative oversize distribution $\theta_e(\ell)$. The value of the nucleation rate B can then be obtained from Eq. 36 and the experimentally measured magma density by using the relation:

$$\mu_3 = \frac{M_T}{\sigma\rho G^3 \tau^4 B} \tag{37}$$

In the present work the calculations have been simplified by the empirical relationship of Eq. 34 with the constants in Table 1. When the experimental data are available in the form of cumulative oversize concentration at various sizes, that is, data sets (ℓ, t) where

$$t(\ell) = \int_{\ell}^{\infty} n(\ell')\, d\ell' \tag{38}$$

Table 2. Values of Constants in Eq. 36

Constant	Values
c_1	1.01491
c_2	0.00238
c_3	0.88572
c_4	1.19280
c_5	0.25666
m	0.48738

then one may directly fit the $t(\ell)$ data to obtain $B\tau$, ϕ, and $G\tau$, since it is readily seen that

$$t(\ell) = \frac{B\tau(\sqrt{(1+2\phi)}-1)}{\phi}\,\theta(\ell/G\tau) \tag{39}$$

As an example of using the above procedure, the data of Tavare et al. (1985) on the crystallization and agglomeration of nickel ammonium sulfate in an MSMPR system were fitted by Eq. 39 to extract the parameters $B\tau$, ϕ, and $G\tau$. For any guessed value of ϕ and $G\tau$, Eq. 34 and the constants in Table 1 provide ($\ell/G\tau$, θ) points at the specific θ values of Table 1. The interpolation package CSAKM in the IMSL library was used to estimate the predicted points ($\ell/G\tau$, θ) at the experimental ℓ's, and for assumed $B\tau$ Eq. 39 provided the predicted $t(\ell)$, which was fitted to its experimental counterpart. For fitting, the constrained minimization package BCONF of the IMSL library was used to minimize the error of $\ln[t(\ell)]$ in a least-square sense. Figure 11 shows the experimental and fitted cumulative oversize distributions. The parameter values extracted from the fitting yielded:

$$B = 1.64\times10^{9}\ \mathrm{L^{-1}\cdot h^{-1}}$$
$$G = 409.2\ \mu\mathrm{m\cdot h^{-1}}$$
$$\phi = 78.81$$

and from these it was estimated that $\beta = 7.71\times10^{-7}\ \mathrm{L\cdot h^{-1}}$. This growth rate is far larger than that estimated by Tavare et al., who obtain $G = 130.8\ \mu\mathrm{m\cdot h^{-1}}$, but this is to be expected since they have assumed length to be conserved in agglomeration instead of mass. This assumption increases the size of an agglomerate in comparison to the mass-conserving case, thereby enhancing the role of agglomeration relative to growth. As a further check of the results, we calculate the predicted magma density using Eqs. 36 and 37 with the above parameters and volume shape factor $\sigma = \pi/6$ and $\rho = 1{,}923\ \mathrm{kg/m^3}$. This

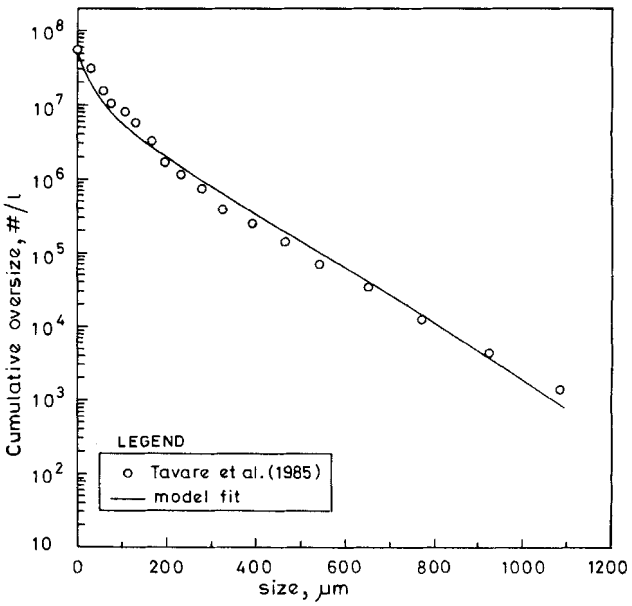

Figure 11. Fit of PBE with constant aggregation kernel to data of Tavare et al. (1985).

yields $M_T = 105$ kg/m^3, which is about 15% higher than the experimental value of 91 kg/m^3 reported by Tavare et al. Considering that the shape factor used is that for spherical particles, the above difference is not significant and may be attributable to the error in this value. As a further basis for comparison, Hounslow's (1990) fit of the same data yielded $B = 1.665 \times 10^9$ L$^{-1}\cdot$h^{-1}, $G = 388$ μm$\cdot$h^{-1} and $\beta_0 = 7.997 \times 10^{-7}$ L$\cdot$h^{-1}, which agrees quite well with the current estimate. However, it may be mentioned that Hounslow's fit extends down to fractional cumulative oversize of about 2×10^{-6} which is unjustifiable in view of its numerical inaccuracy below about 10^{-3} as shown above. Perhaps this accounts for the slightly lower growth rate estimated by Hounslow, as his procedure overpredicts at larger sizes. In the fit obtained here the present approach, which is accurate down to cumulative oversize fraction of 10^{-5}, was applied only to the data above this level. Besides the virtue of greater accuracy, however, the present procedure has the advantage that the predicted θ-ℓ relationship is easily obtained by Eq. 34 and the constants in Table 1.

It may be mentioned that the constant aggregation kernel model solved here is only an approximation to the real situation. In practice, the aggregation frequency is likely to change with size, and hence the experimental oversize data may be actually better fitted by Hounslow's solution when the real kernel causes the density and oversize at large sizes to be higher than for the constant kernel case. However, the better fit should not be construed as an indication of better accuracy of the solution.

As another example of using Eqs. 34-39, Figures 12 and 13 show the fit of some of our own (unpublished) data on the continuous precipitation of calcium carbonate by the double-decomposition reaction between calcium nitrate and sodium carbonate at 25°C and $\tau = 6$ min. Details of the experimental apparatus and technique are provided elsewhere (Chakraborty, 1992; Chakraborty and Bhatia, 1992). The particle size distribution was measured by an on-line Galai CIS-1 laser monitor. The instrument works on the "time of transition" principle and measures the total number concentration and distribution for particles above 0.5 μm with good reproducibility, and confidence level over 95%.

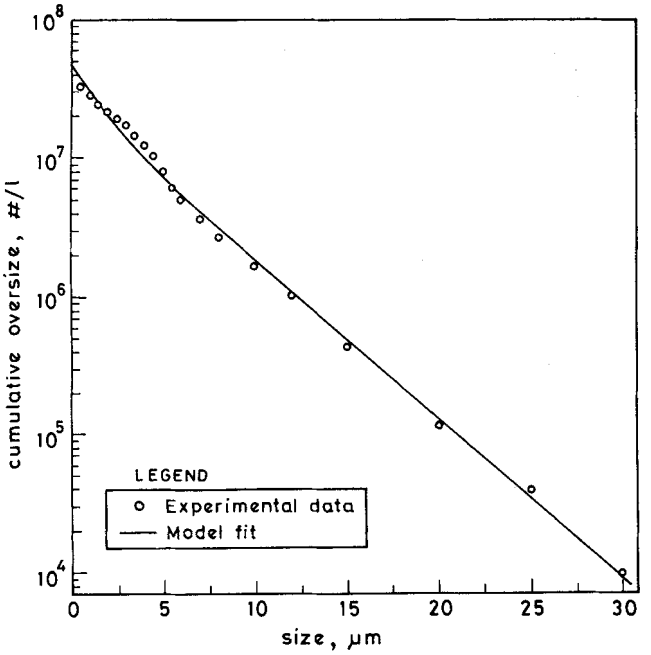

Figure 12. Fit of PBE to cumulative oversize data for precipitation of calcium carbonate at high CO_3^{--}/Ca^{++} ratio (Chakraborty, 1992).

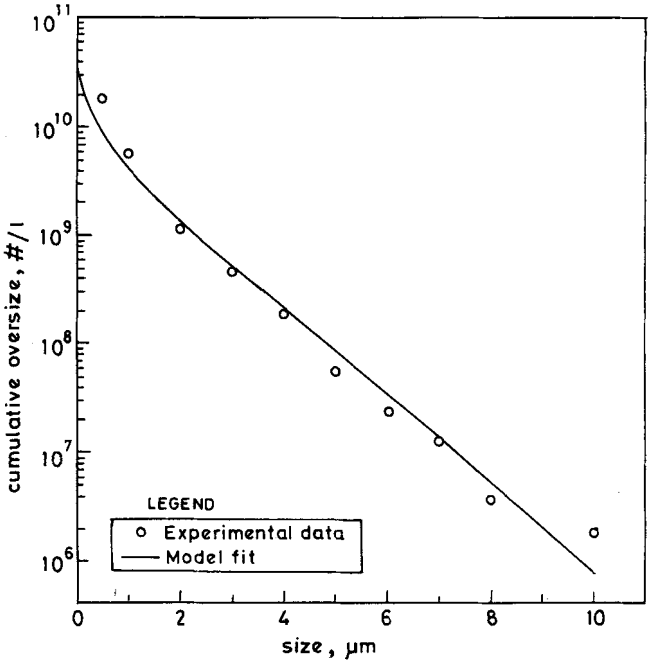

Figure 13. Fit of PBE to cumulative oversize data for precipitation of calcium carbonate under nearly stoichiometric conditions (Chakraborty, 1992).

In Figures 12 and 13, the measured cumulative oversize data were fitted by the predicted $t(\ell)$ to estimate the values of B, G and ϕ. This yielded $B = 9.35 \times 10^8$ L$^{-1}\cdot$h^{-1}, $G = 35.59$ μm$\cdot$h^{-1}, and $\phi = 3.27$ for the data of Figure 12, while $B = 1.48 \times 10^{12}$ L$^{-1}\cdot$h^{-1}, $G = 9.78$ μm$\cdot$h^{-1}, and $\phi = 29.87$ for Figure 13. It may be noted that Figure 13 does show a small systematic curvature around the predicted curve, but this could be correlated qualitatively with the presence of more than one form of $CaCO_3$ in the precipitate. Microscopic examination of the precipitated particles showed the primary particles to be predominantly spherical (corresponding to vaterite) with small amounts of cubical ones (calcite) for the conditions corresponding to Figure 12. It also showed a relatively small population of aggregates consistent with the low value of $\phi = 3.27$ for this run. However, for Figure 13 the particles were mostly cubical with smaller amounts of the spherical variety, but the agglomerate population was indeed high consistent with larger estimate of $\phi = 29.87$.

It is well known (Groot and Duyvis, 1966) that calcite is relatively much slower in growth than any other polymorph of $CaCO_3$ in the presence of trace amounts of Mg^{+2} (which exist in our system). Thus, in a mixture, in which vaterite is relatively more numerous, the slow-growing calcite restricted to the lower side of the distribution, where the density is the highest, will be overshadowed by the more dominant polymorph and may not significantly affect the overall distribution. This accounts for the relatively better fit in Figure 12. On the

other hand, in a mixture, in which calcite is relatively more numerous overall, the much faster growing vaterite may have a population density comparable to that of calcite at large sizes, where the density of the latter will be small. Thus, for Figure 13, the distribution may be affected by both of the growth rates. The curvature is also similar to that normally associated with growth rate dispersion (Berglund and deJong, 1990), suggesting that for this case an improvement may be obtained by accounting for this effect. However, it is not immediately clear as to what growth rate must be assigned to the agglomerates when the primary particles comprise polymorphs with different growth rates. Modeling aggregative precipitation for such a system is an outstanding problem that has not received attention yet.

Acknowledgment

This research was supported by a grant (No. DST/III-4[17]/86-ET) from the Department of Science and Technology.

Notation

A = operator
a_i, a_i' = constants
b_i, b_i' = constants
B = nucleation rate per unit slurry volume
$C_1 - C_5$ = constants, defined in Table 2
C = constant
$d_1 - d_5$ = constants, defined in Table 1
f = nonhomogeneous term, Eq. 1
G = growth rate
ℓ = particle size
L = maximum moment
m = constant, Table 2
M = number of quadrature points
M_T = slurry density
$n(y)$ = population density
N = number of terms in expansion
N_1 = number of equations in Hounslow's method
N_s = number of elements
p = constant, Table 1
$q(y)$ = dimensionless population density, $n(\ell)G/B$
$q^*(y)$ = approximate solution
$q_L(y)$ = Eq. 17
$q_u(y)$ = Eq. 20
$t(\ell)$ = cumulative oversize number concentration at size ℓ
x = quadrature points for Gauss-Legendre quadrature
y = $\ell/G\tau$
y_{a_i} = lower limit of ith interval
Δy_i = size of ith interval, $y_{a_{i+1}} - y_{a_i}$
z = quadrature points for Gauss-Laguerre quadrature

Greek letters

α = Eq. 12
β = constant aggregation kernel
Δ = fractional error in evaluation of integral in Eq. 30
μ_j = jth moment of $q(y)$, Eq. 16
ϕ = agglomeration parameter, $\beta B\tau^2$
φ_i, φ_i' = polynomial sequences
ρ = particle density of precipitate
σ = shape factor
τ = residence time
$\theta(y)$ = fractional oversize distribution
$\bar{\theta}(y)$ = true fractional oversize distribution

Literature Cited

Berglund, K. A., and E. J. deJong, "The Calculation of Growth and Nucleation Kinetics from MSMPR Crystallizer Data Including Growth Rate Dispersion," *Sep. Tech.*, **1**, 38 (1990).

Chakraborty, D., "Kinetics of Precipitation of Calcium Carbonate," PhD Diss., Indian Inst. of Technol., Bombay, in progress (1992).

Chakraborty, D., and S. K. Bhatia, "Studies of Continuous Reaction Precipitation," Project Report (No. DST/III-4[17]/86-ET, submitted to Dept. of Science and Technology, India (1992).

Chang, R. Y., and M. L. Wang, "Modeling the Batch Crystallization Process via Shifted Legendre Polynomials," *Ind. Eng. Chem. Process. Des. Dev.*, **23**, 463 (1984a).

Chang, R. Y., and M. L. Wang, "Shifted Legendre Function Approximation of Differential Equations: Application to Crystallization Processes," *Comp. Chem. Eng.*, **8**, 125 (1984b).

Dennery, P., and A. Krzywicki, *Mathematics for Physicists*, Harper and Row, New York (1967).

Finlayson, B. A., *Method of Weighted Residuals and Variational Principles*, Academic Press, New York (1972).

Finlayson, B. A., *Nonlinear Analysis in Chemical Engineering*, McGraw-Hill, New York (1980).

Gelbard, F., and J. H. Seinfeld, "Numerical Simulation of the Dynamic Equation for Particulate Systems," *J. Comp. Phys.*, **28**, 357 (1978).

Groot, K. De., and E. M. Duyvis, "Crystal Form of Precipitated Calcium Carbonate as Influenced by Adsorbed Magnesium Ions," *Nat.*, **212**, 183 (1966).

Hostomsky, J., and A. G. Jones, "Calcium Carbonate Crystallization, Agglomeration and Form During Continuous Precipitation from Solution," *J. Phys. D: Appl. Phys.*, **24**, 165 (1991).

Hounslow, M. J., "A Discretized Population Balance for Continuous Systems at Steady State," *AIChE J.*, **36**, 106 (1990).

Hounslow, M. J., R. L. Ryall, and V. R. Marshall, "Modeling the Formation of Urinary Stones," CHEMICA, 1097, Sydney, Australia (1988).

Lamey, M. D., and T. A. Ring, "The Effects of Agglomeration in a Continuous Stirred Tank Crystallizer," *Chem. Engng. Sci.*, **41**, 1213 (1986).

Marchal, P., R. David, J. P. Klein, and J. Villermaux, "Crystallization and Precipitation Engineering: I. An Efficient Method for Solving Population Balance in Crystallization with Agglomeration," *Chem. Eng. Sci.*, **43**, 59 (1988).

Ramkrishna, D., "On Problem-Specific Polynomials," *Chem. Eng. Sci.*, **28**, 1362 (1973).

Sampson, K. J., and D. Ramkrishna, "A New Solution to the Brownian Coagulation Equation through the Use of Root Shifted Problem-Specific Polynomials," *J. Coll. Int. Sci.*, **103**, 245 (1985).

Singh, P. N., and D. Ramkrishna, "Transient Solution of the Brownian Coagulation Equation by Problem-Specific Polynomials," *J. Coll. Int. Sci.*, **53**, 214 (1975).

Singh, P. N., and D. Ramkrishna, "Solution of Population Balance Equations by MWR," *Comp. Chem. Eng.*, **1**, 23 (1977).

Smit, D. J., Dept. of Chemical Engineering, Univ. of Cambridge, personal communication (1991).

Tavare, N. S., M. B. Shah, and J. Garside, "Crystallization and Agglomeration Kinetics of Nickel Ammonium Sulphate in an MSMPR Crystallizer," *Powder Technol.*, **44**, 13 (1985).

Manuscript received Sept. 23, 1991, and revision received Feb. 28, 1992.